Evidence for internal structures of spiral turbulence

S. Dong*
Department of Mathematics, Purdue University, West Lafayette, Indiana 47907, USA
(Received 19 March 2009; revised manuscript received 19 November 2009; published 22 December 2009)

We present several observations into spiral turbulence in a Taylor-Couette geometry gained through a three-dimensional direct numerical simulation. Conditionally averaged flow statistics show the persistence of an azimuthal gradient of the mean flow across both the turbulent and laminar spirals, and distinct distribution features of the turbulent intensity. The data provide a physical picture qualitatively different from the existing model of spiral turbulence. Certain aspects of the spiral pattern are observed to bear similarities to the stationary laminar-turbulent pattern in plane Couette flow.

DOI: 10.1103/PhysRevE.80.067301 PACS number(s): 47.20.Qr, 47.27.−i, 47.32.Ef

The coexistence of turbulent and laminar domains in space and time is one of the most fascinating phenomena in fluid dynamics. Spatiotemporal intermittency and pattern formation in such flows have been observed for a variety of systems [1]. Particularly intriguing is the spiral turbulence regime (barber-pole pattern) in the Taylor-Couette setting where intertwined helical turbulent and laminar stripes propagate between counter-rotating concentric cylinders [2,3]. On the largest scale spiral turbulence is observed to relate to a finite-wavelength modulation of turbulent intensities, and aspects of the spiral pattern can be qualitatively described by model equations [3]. In other systems related patterns are the stationary laminar-turbulent pattern in plane Couette flow and the torsional flow between a stationary and a rotating disk [4].

In this Brief Report we present several observations into spiral turbulence gained from a three-dimensional (3D) direct numerical simulation. By employing conditional averaging techniques, we have obtained flow statistics of a single turbulent or laminar spiral for a range of Reynolds numbers. The data demonstrate large-scale spatial variations of the flow internal to the turbulent and laminar spirals, and unique characteristics in the mean flow and turbulent intensity.

We consider the incompressible flow between two concentric cylinders with periodic boundary conditions in the axial direction. The cylinder axis is aligned with the z axis of the coordinate system. The geometry is characterized by the radius ratio $\eta = R_i/R_o$ (R_i and R_o are, respectively, the inner- and outer-cylinder radii) and the aspect ratio $\Gamma = L_z/d$ (L_z is the domain axial dimension and d is the gap width, with $d = R_o - R_i$). The inner cylinder rotates counterclockwise (viewing toward the $-z$ direction) at an angular velocity Ω_i, and the outer cylinder rotates clockwise at an angular velocity Ω_o. All length variables are normalized by R_i, the velocity by a natural velocity U_d (leading to $\Omega_o R_o/U_d = -1.08$), and the pressure by ρU_d^2 (ρ is the fluid density). The inner- and outer-cylinder Reynolds numbers are defined by $\mathrm{Re}_i = \Omega_i R_i d/\nu$ and $\mathrm{Re}_o = \Omega_o R_o d/\nu$ (ν is the kinematic viscosity).

Our computational algorithms have been documented in detail in previous works [5]. In brief, we numerically solve the 3D Navier-Stokes equations employing a Fourier spectral expansion of flow variables along the axial direction and a high-order spectral-element discretization of the annular domain. The effectiveness of spectral-element-based approach has been evidenced in previous studies [6]. The time discretization is based on a stiffly stable scheme [7]. No-slip boundary conditions are applied on the inner and outer cylinders to reflect their rotation velocities.

We consider a radius ratio $\eta = 0.89$, comparable to those of previous experiments [2,3]. We fix Re_o at -1375 and vary Re_i between 530 and 900. In light of the computational cost, we aim to simulate only one complete turbulent spiral. For this purpose we consider several aspect ratios ranging from $\Gamma \approx 6$ to 25. At $\Gamma \approx 12$ and higher we have observed complete turbulent spirals, while at a low Γ no spiral can be observed. Results reported herein are for $\Gamma = 25.1$. To ensure convergence of the simulation results, we have varied the resolutions systematically. The number of Fourier planes in the axial direction is varied between 384 and 512. In the annular domain 640 quadrilateral spectral elements are employed; and the element order is varied from 6 to 9. By comparing profiles of the time-averaged mean and root-mean-square (rms) fluctuation velocities at different resolutions, we have confirmed the convergence of our simulation results. Our application code has been extensively validated for Taylor-Couette turbulence by comparing the computed flow quantities with those determined from experiments; see [5] for details on the validations. We have also compared the turbulent fraction of spiral turbulence obtained from the current simulation and the experiment of Goharzadeh and Mutabazi [2], and good agreement has been observed.

We start by exploring the Reynolds number dependence of the patterns. Figure 1(a) is a composite plot of a long simulation spanning $530 \le \mathrm{Re}_i \le 900$, with Re_i increased in discrete steps and Re_o fixed at -1375. Shown are the stable patterns at each Re_i (transients at the change in Re_i are not shown). We record time histories of the velocity over points along a line parallel to the z axis and fixed in the midgap. Plotted are the azimuthal velocity contours in spatial-temporal (z-t) plane. Distinct patterns can be identified with increasing Re_i. At $\mathrm{Re}_i = 530$ turbulent patches (bursts) are observed to emerge from the laminar background, persist for a while, and then disappear into the flow; some aspects of the turbulent bursts are described in [8]. At $\mathrm{Re}_i = 560$, we mostly observe complete spirals which appear quite regular; however, from time to time the spiral becomes broken, with two or more pieces. At $\mathrm{Re}_i = 611-700$, one can observe regular turbulent-laminar spirals, characterized by regularly spaced

*sdong@math.purdue.edu

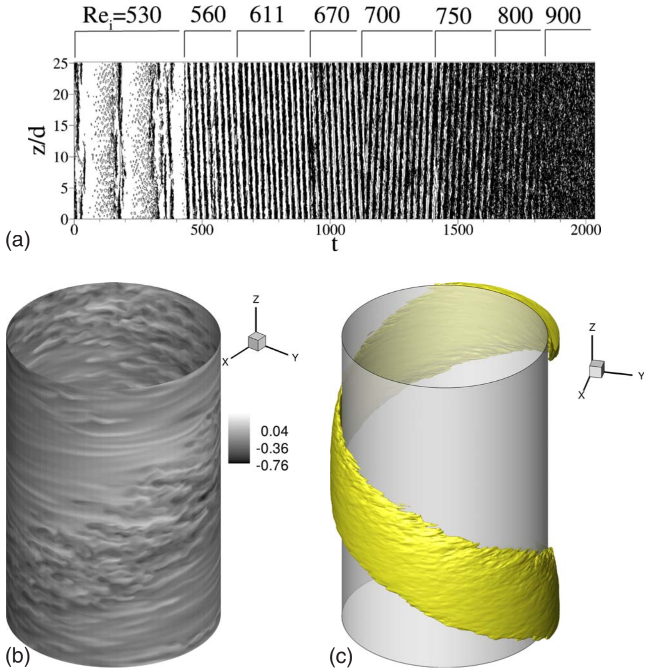

FIG. 1. (Color online) Turbulent-laminar patterns. (a) Contours of azimuthal velocity in spatial (z) and temporal (t) planes. Time evolves horizontally with changes in Re_i indicated at the top. Dark and blank regions, respectively, represent turbulent and laminar flows. (b) Instantaneous azimuthal velocity contours in a cylindrical grid surface showing the turbulent spiral at $\mathrm{Re}_i=700$. (c) Isosurface of conditionally averaged rms velocity magnitude $u'/U_d=0.14$ ($\mathrm{Re}_i=611$).

inclined stripes in Fig. 1(a). As Re_i increases to 750 and 800, the pattern becomes less recognizable, and turbulent fluctuations increasingly dominate the flow. At $\mathrm{Re}_i=900$ the entire flow becomes turbulent, and no apparent large-scale pattern can be discerned.

We next focus on Re_i values with well-defined spiral patterns. Figure 1(b) shows a typical turbulent-laminar spiral pattern from the simulation. We plot here the instantaneous azimuthal velocity contours in a grid surface (essentially cylindrical) near the midgap. One can observe that the turbulent and laminar regions form right-handed spirals. This plot is reminiscent of the photographs of turbulent spirals in previous experiments [2]. For all Re_i considered here, the spiral pattern rotates clockwise, in the same direction as the outer cylinder, a point consistent with previous experiments [2,3]. Left-handed spirals have also been observed (e.g., at $\mathrm{Re}_i=611$). In current simulations, because both Re_i and Re_o are fixed and $|\mathrm{Re}_o|$ is low, we do not observe both types of spirals simultaneously in stable coexistence (transient coexistence has been observed). Andereck *et al.* [2] noted that stable coexistence of both types might occur for large Re_o values and with rapid increase in Re_i.

To explore the statistical features of turbulent spirals, we have employed two types of conditional averaging techniques. The first type involves a whole-field averaging. Specifically, for a given Re_i the rotation period of the spiral pattern is first determined by a Fourier transform of the velocity history data. The flow field at an instant t_0 is considered as the base flow. We consider a moving coordinate system which coincides with the laboratory system at t_0 and revolves around the z axis at the same angular frequency as the pattern. At time t, we rotate the flow field back to the base configuration (i.e., that at t_0) based on $(t-t_0)$ and the angular frequency. The rotated field is then accumulated to the base flow for averaging. With this technique the spiral pattern is essentially frozen in space, and its key statistical features can be exposed. Figure 1(c) shows an isosurface of the conditional rms velocity magnitude u'/U_d, where $u'=\sqrt{u_r'^2+u_\theta'^2+u_z'^2}$ (u_r', u_θ, and u_z' denote the conditional rms velocity in radial, azimuthal, and axial directions). The isosurface reflects the shape of the 3D interface between the turbulent and laminar spirals. The domain enclosed by the isosurface marks the turbulent region, a helical band wrapping around the inner cylinder with certain subtle features. For example, its leading edge [the lower edge in Fig. 1(c) as it rotates clockwise] is radially nearer to the outer cylinder, while the trailing edge is closer to the inner one, a topological feature that will become clearer later.

The other type is a spatiotemporal conditional averaging. It is applied to the spatial-temporal data [see Fig. 1(a)], which provides a velocity time history at each axial location z. The turbulent (laminar) phases in the velocity histories at different z's are not aligned in time, thus leading to the inclined stripes in Fig. 1(a). For a given Re_i, the average inclination angle of the stripe pattern in Fig. 1(a) is first determined, which provides the phase-shift information. The velocity history at a location z_0 is considered as the base history. We then shift in time the velocity history at any z to align the turbulent phases with the base history, based on $(z-z_0)$ and the stripe average inclination angle. The shifted data are accumulated to the base velocity history for averaging. This results in a velocity history, conditionally averaged over the points along the z direction. It is a periodic signal, with the rotation period of the spiral pattern as its period. We then shift in time this conditionally averaged velocity history and average over different periods.

The conditionally averaged statistics indicate the existence of internal structures of the spiral turbulence. First, an azimuthal velocity gradient, $\partial\langle u_\theta\rangle/r\partial\theta$ ($\langle u_\theta\rangle$ denotes conditional mean azimuthal velocity, and r and θ are radial and azimuthal coordinates), persists across the turbulent and laminar spirals. Figure 2(a) shows several periods of the spatiotemporally averaged conditional mean and rms azimuthal velocity, together with an instantaneous base history at z_0. Alternating turbulent and laminar phases can be clearly distinguished. Most striking is the large systemic variation of the conditional mean velocity in the turbulent and laminar phases. Note that the onset of turbulent phase corresponds to the passing of the leading edge of a turbulent spiral over a fixed point in space, and the end of turbulent phase corresponds to the passing of the trailing edge. Therefore, Fig. 2(a) indicates that along the azimuthal direction the mean velocity experiences a substantial variation across the turbulent and laminar spirals. The trailing edge of a turbulent spiral has a notably higher mean velocity magnitude than the leading one. It is the reverse for a laminar spiral. This observation applies to all Re_i studied here with well-defined spiral patterns.

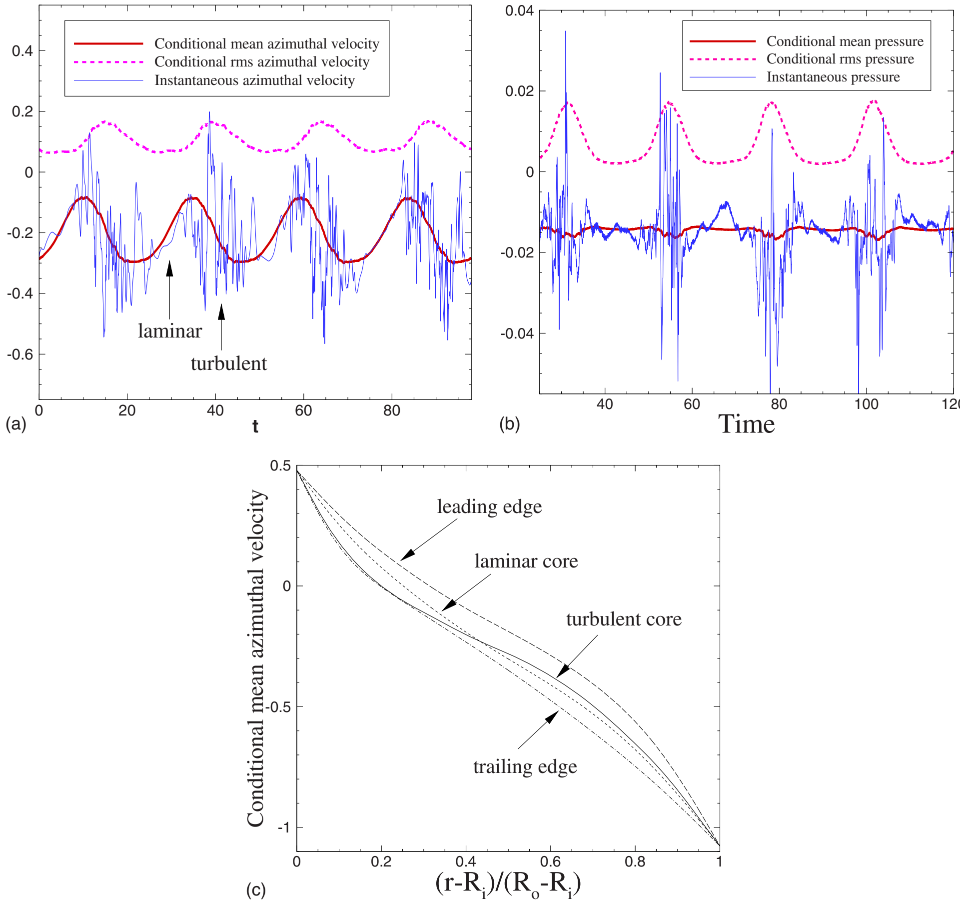

FIG. 2. (Color online) Spatiotemporal conditional mean [red (dark) solid line], rms (purple dashed line), and instantaneous azimuthal [blue (light) solid line] (a) velocity (Re_i=700) and (b) pressure (Re_i=611) in the midgap. (c) Conditional mean azimuthal velocity profiles at turbulent and laminar spiral cores, and leading and trailing edges of turbulent spiral (Re_i=611).

This observation has a connection to the Hayot and Pomeau model [9] of spiral turbulence. When modeling the coexistence of stable laminar and turbulent domains of spiral turbulence using the Ginzburg-Landau equation, Hayot and Pomeau introduced a crucial nonlocal term, which leads to a stable domain structure, whereas without such a term no stable domains coexist. The model is based on two crucial assumptions: (1) the azimuthal dependence of the mean azimuthal velocity and (2) the presence of a mean azimuthal pressure gradient. It concludes that (1) the mean azimuthal pressure gradient has large magnitudes in both the laminar and turbulent regions and (2) a large Poiseuille flow component is present in the mean azimuthal velocity due to the mean pressure gradient. The large Poiseuille component has also been argued by Hegseth *et al.* [3].

Our observation above is consistent with the first assumption that underpins the Hayot and Pomeau model. However, simulation results provide a physical picture qualitatively different than the model. To examine the pressure, we show in Fig. 2(b) the spatiotemporal conditional mean and rms pressure, and the instantaneous pressure history at z_0. The conditional mean pressure is essentially constant in the laminar phase and exhibits notable variations only in the turbulent phase. That is, the mean pressure is essentially constant across the laminar spiral and has a significant azimuthal gradient only in the turbulent spiral region. This is very different from the conclusion of the Hayot and Pomeau model. Figure 2(c) shows profiles (across the cylinder gap) of the conditionally averaged mean azimuthal velocity at several azimuthal locations: the leading edge, trailing edge, and the core of the turbulent spiral, as well as the core of the laminar spiral. Examination of these mean velocity profiles shows that the variation of the mean azimuthal velocity along the azimuthal direction has a rather involved characteristic and is not of Poiseuille flow type. Significant changes in the mean velocity tend to occur in only part of the cylinder gap. For example, from the turbulent spiral core to the trailing edge the mean azimuthal velocity has a significant increase in magnitude in the outer half of the gap, but essentially no change toward the inner half, while from the leading edge to the turbulent core the largest change occurs in the inner portion of the gap. Therefore, our simulation results suggest that significant mean azimuthal pressure gradient exists only in the turbulent spiral region, and that the azimuthal Poiseuille flow component from the Hayot and Pomeau model is not evident.

The second main observation about spiral turbulence is that the cores of turbulent and laminar spirals are demarcations of axially opposite flows in the mean sense. The mean axial flow tends to be away from the core of a turbulent spiral and toward the cores of adjacent laminar spirals. This is demonstrated in Figs. 3(a) and 3(b), which, respectively, show contours of the conditional mean axial velocity and conditional rms velocity magnitude u'/U_d in a radial-axial plane. One can observe that the core of the turbulent spiral marks an interface; on both sides the flow tends to be away from this interface. Similarly, the laminar spiral core marks another interface at which flows on both sides tend to be

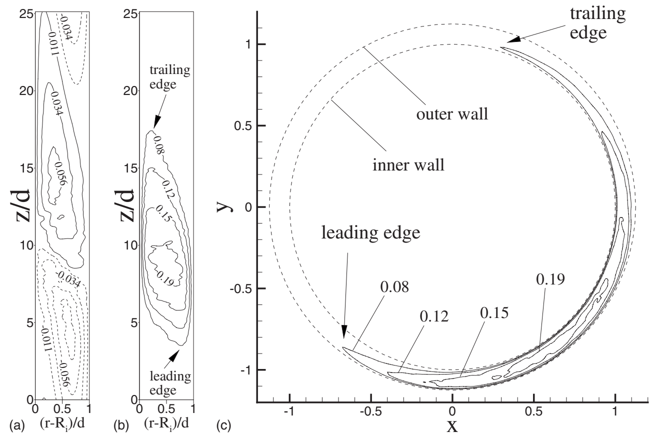

FIG. 3. Contours of (a) conditional mean axial velocity $\langle u_z \rangle / U_d$, (b) conditional rms velocity magnitude u'/U_d in a radial-axial plane, and (c) of u'/U_d in a horizontal plane (Re_i=611).

toward each other. This observation is generic to all Re_i studied here with both left- and right-handed spirals. It is, however, somewhat counterintuitive. For example, because a left-handed turbulent spiral propagates axially along the $-z$ direction, intuitively the leading and trailing edges would have a negative mean axial velocity. This is true for the leading edge. Contrary to intuition, however, the trailing edge has actually a positive mean axial velocity. A similar situation occurs to right-handed spirals.

Third, the distribution of turbulent intensity exhibits a different characteristic in spiral turbulence than in fully developed turbulence. This is demonstrated in Figs. 3(b) and 3(c) which show contours of u'/U_d in a horizontal x-y plane at midheight of the cylinder. In spiral turbulence the most energetic intensity appears at the core of turbulent spiral, toward the middle of the gap. In contrast, in fully developed Taylor-Couette turbulence at high Reynolds numbers the strongest turbulent intensity tends to be located near both walls rather than in the midgap [5]. Figures 3(b) and 3(c) also clearly illustrate our previous point that the leading edge of the turbulent spiral has a proximity to the outer wall while the trailing edge has a proximity to the inner one, a point also noted by Atta [2].

The observations discussed above for spiral turbulence can be contrasted with, and oftentimes, can find their counterparts in the stationary turbulent-laminar pattern in plane Couette flow. Here, we refer to the work of Barkley and Tuckerman [10], which provides a detailed analysis of the mean flow and force balance of the patterns in plane Couette flow. The negligible mean pressure gradient in laminar spiral region [Fig. 2(b)], the phase difference between mean and rms velocities as shown in Fig. 2(a), and the sense of mean axial flow relative to spiral cores [Fig. 3(a)] are consistent with the data for plane Couette flow [10]. The similarity between spiral turbulence and the pattern in plane Couette flow is noted by several studies (see Prigent *et al.* [3], among others). Prigent *et al.* experimentally showed the long wavelengths in both types of patterns.

On the other hand, we also note marked differences between the two patterns. First, in spiral turbulence due to wall curvature and the fact that the pattern is propagating, a profound asymmetry exists between the leading and trailing parts of the pattern, regarding their shape, turbulent intensity distribution, and wall proximity; see Fig. 3 and also Atta [2]. In plane Couette flow no such asymmetry exists between the pattern boundaries. Second, in the counter-rotating setting of spiral turbulence, the region near inner wall is linearly unstable and more susceptible to instabilities. This leads to an asymmetry in flow features near the two walls. This asymmetry has been discussed at length in large-gap simulations [5]. It also imprints on the spiral turbulence. For example, the mean velocity profile in the turbulent spiral core is asymmetric with respect to the two walls [Fig. 2(c)]; in contrast, the plane Couette flow is linearly stable everywhere, and the mean profile in the center of turbulent region is symmetric between the two walls [10].

The author gratefully acknowledges the support from NSF and the TeraGrid.

[1] M. Cross and P. Hohenberg, Rev. Mod. Phys. **65**, 851 (1993).
[2] D. Coles, J. Fluid Mech. **21**, 385 (1965); C. Van Atta, *ibid.* **25**, 495 (1966); C. Andereck, S. Liu, and H. Swinney, *ibid.* **164**, 155 (1986); H. Litschke and K. Roesner, Exp. Fluids **24**, 201 (1998); A. Goharzadeh and I. Mutabazi, Eur. Phys. J. B **19**, 157 (2001).
[3] J. J. Hegseth, C. D. Andereck, F. Hayot, and Y. Pomeau, Phys. Rev. Lett. **62**, 257 (1989); A. Prigent, G. Gregoire, H. Chate, O. Dauchot, and W. van Saarloos, *ibid.* **89**, 014501 (2002).
[4] D. Barkley and L. S. Tuckerman, Phys. Rev. Lett. **94**, 014502 (2005); A. Cros and P. L. Gal, Phys. Fluids **14**, 3755 (2002).
[5] S. Dong, J. Fluid Mech. **587**, 373 (2007); **615**, 371 (2008).
[6] S. Dong *et al.*, J. Fluid Mech. **569**, 185 (2006); S. Dong, G. S. Triantafyllou, and G. E. Karniadakis, Phys. Rev. Lett. **100**, 204501 (2008).
[7] G. Karniadakis, M. Israeli, and S. Orszag, J. Comput. Phys. **97**, 414 (1991).
[8] K. Coughlin and P. S. Marcus, Phys. Rev. Lett. **77**, 2214 (1996); P. W. Colovas and C. D. Andereck, Phys. Rev. E **55**, 2736 (1997).
[9] F. Hayot and Y. Pomeau, Phys. Rev. E **50**, 2019 (1994).
[10] D. Barkley and L. Tuckerman, J. Fluid Mech. **576**, 109 (2007); *IUTAM Symposium on Laminar-Turbulent Transition and Finite Amplitude Solutions* (Springer, New York, 2005), pp. 107–127; J. J. Hegseth, Phys. Rev. E **54**, 4915 (1996).